UDK 669.017.12:537.226.5
Original scientific article/Izvirni znanstveni članek

ISSN 1580-2949
MTAEC9, 56(2)149(2022)

STRUCTURAL AND ELASTIC PROPERTIES OF $AgNi_{10}$ ALLOY STUDIED WITH AB-INITIO CALCULATIONS

STRUKTURNE IN ELASTIČNE LASTNOSTI ZLITINE $AgNi_{10}$, PREUČEVANE S POMOČJO KVANTNO-MEHANSKIH (*AB INITIO*) IZRAČUNOV

Jide Liu[1], Xue Wang[2], Xiaoming Du[2*], Ming Xie[3], Jinguo Li[1], Shangqiang Zhao[3], Yizhou Zhou[1], Qiao Zhang[3], Jiheng Fang[3]

[1]Institute of Metal Research, Chinese Academy of Sciences, Shenyang, 110016, China
[2]School of Materials Science and Engineering, Shenyang Ligong University, Shenyang 110159, China
[3]Kunming Guiyan New Material Technology Co., Ltd.Kunming, 650106, China

Prejem rokopisa – received: 2022-01-22; sprejem za objavo – accepted for publication: 2022-02-15

doi:10.17222/mit.2022.377

First-principles calculations based on density functional theory (DFT) are used to calculate the structural, elastic and thermodynamic properties of the supersaturated solid-solution $AgNi_{10}$ alloy, applied mainly to electrical contact materials. In this work, for the exchange-correlation energy, the generalized gradient approximation (GGA) functional is used. The calculated structural and electronic properties of supersaturated solid-solution $AgNi_{10}$ alloys show that the occupation of Ni in the Ag lattice is ordered. All single-crystal elastic stiffness constants of the energetically and mechanically optimized stable $AgNi_{10}$ model are calculated using the finite strain method and using the Voigt-Reuss-Hill approximation. Various anisotropic indices like the universal anisotropic index, shear anisotropic index, directional dependence of Young's modulus, bulk modulus and others are calculated to study the elastic anisotropy. The strong anisotropy in the elastic properties of $AgNi_{10}$ was confirmed. Phonon dispersions were carried out, showing that the $AgNi_{10}$ crystal has dynamic stability. The Debye temperature is calculated from the elastic data by estimating the average sound velocity in the $AgNi_{10}$. Furthermore, the vibrational thermodynamic properties (free energy, enthalpy, entropy and heat capacity) of $AgNi_{10}$ are obtained successfully.

Keywords: $AgNi_{10}$ alloy, ab initio calculations, elastic anisotropy, thermodynamic properties

Avtorji v članku opisujejo osnovne izračune, ki temeljijo na teoriji funkcionalne gostote (DFT; Density Functional Theory) za izračunavanje strukturnih, elastičnih in termodinamskih lastnosti prenasičene trdne raztopine zlitine $AgNi_{10}$, ki se pretežno uporablja kot material za električne kontakte. V tem delu so avtorji uporabili izmenjalno-korelacijsko energijo, posplošeno s funkcionalno gradientno aproksimacijo (GGA). Izračuni strukturnih in elektronskih lastnosti prenasičene trdne raztopine zlitine $AgNi_{10}$ so pokazali, da prihaja do urejene zasedenosti Ni atomov v Ag rešetki. Z metodo končne deformacije in uporabo Voigt-Reuss-Hill aproksimacije so izračunali vse elastične konstante togosti monokristala za energetsko in mehansko optimizirano stabilni model $AgNi_{10}$. Različne anizotropne pokazatelje kot so: univerzalni indeks anizotropije, indeks strižne anizotropije, odvisnost Youngovega modula od smeri, volumski modul in druge, so avtorji izračunali s pomočjo študije elastične anizotropije. Potrdili so močno anizotropijo elastičnih lastnosti zlitine $AgNi_{10}$. Izvedli so fononsko disperzijo in pokazali, da je kristal $AgNi_{10}$ dinamično stabilen. Izračunali so Debyevo temperaturo iz elastičnih podatkov z ocenitvijo povprečne hitrosti zvoka v $AgNi_{10}$. Nadalje so avtorji še uspešno določili vibracijske termodinamične lastnosti $AgNi_{10}$ in sicer: prosto energijo, entalpijo, entropijo in toplotno kapaciteto.

Ključne besede: zlitina $AgNi_{10}$, kvantno-mehanski (*ab initio*) izračuni, elastična anizotropija, termodinamične lastnosti

1 INTRODUCTION

Ag-Ni binary alloy systems are widely used in electrical contact materials due to the high conductibility of electricity and heat, low and stable contact resistance. However, the resistance of silver-based alloys to arc erosion and splashing is weak. How to improve the welding resistance and wear resistance on the premise of reducing the conductivity, so as to improve the service life of materials used in electrical contact friction pairs, is a subject worthy of research.[1–4]

Under equilibrium conditions, the mixing entropy of solid Ag and Ni is 15 kJ/mol, and the mutual solubility is very small (the maximum solid solubility of Ni in Ag is x_{Ni} = 0.2 % at nearly 960 °C, while Ag can only be dissolved in Ni by x_{Ag} = 1 % at the monotectic temperature 1435 °C).[5,6] During past decades, employing various non-equilibrium techniques, such as mechanical alloying, liquid quenching, and ion-beam mixing, a number of metastable phases, either in the amorphous state or in the crystalline state, were produced in Ag-Ni binary metallic systems. Ricci-Bitti, Tsaur and others obtained supersaturated Ag-Ni films at room temperature by laser coating and ion-beam sputtering, respectively.[7,8] Xu et al. studied the preparation of Ni-Ag supersaturated powder by mechanical alloying.[9] He and Ma argued that the icosahedral order dominated the structure of the Ag-Ni amorphous phase.[10] The structural stability and characteristics of metastable phases formed in the immiscible fcc-hcp or fcc-fcc metallic systems have been studied not only by

*Corresponding author's e-mail:
du511@163.com

experimental means, but also by theoretical modelling. For instance, He et al. have studied the amorphous structures in the Ag-Ni system by vapor quenching and molecular dynamics simulation.[11] Alonso et al. proposed a semi-empirical method to calculate the free-energy diagram of the binary metallic systems.[12]

For the Ag-Ni system, although some experimental studies on the metastable binary alloys have been reported in the literature, there are very few theoretical studies on such a system. Accordingly, more investigations should be carried out to clarify the structural stability and characteristics of the metastable phases formed in an immiscible metallic system. With the development of computational technology, a first-principles calculation has also been employed to study the structural phase transition and characteristics of the metastable alloys at an atomic level. Since there is no equilibrium compound in the immiscible Ag-Ni system, very few experimental data are available for constructing the model. The present study is, therefore, dedicated to investigating the structural stability and the characteristics of the Ag-Ni phases by first-principles calculation, which is carried out to acquire some structural, physical and mechanical properties.

2 EXPERIMENTAL PART

The first-principles calculation is based on the well-established Quantum-ESPRESSO program package.[13] In the package, the calculations are conducted in a plane-wave basis, using fully nonlocal Vanderbilt-type ultrasoft pseudopotentials to describe the electron–ion interaction[14], which allows the use of a moderate cut off for the construction of the plane-wave basis for the transition metals. In the calculation, the exchange and correlation items are described by the generalized-gradient approximation (GGA) proposed by Perdew and Wang.[15] The integration in the Brillouin zone is made on special *k* points determined according to the Monkhorst–Pack scheme.[16] The cut-off energy for plane-wave expansions was determined as 400 eV after convergence tests. The convergence criteria for geometry optimization were as follows: electronic self-consistent field (SCF) tolerance less than 5.0×10^{-5} eV/atom, Hellmann–Feynman force below 0.1 eV/nm, maximum stress less than 0.05 GPa and displacement within 2.0×10^{-5} nm. Convergence with respect to the *k*-point sampling for the Brillouin zone (BZ) integration was tested independently on the phases using regular meshes of increasing density. The tests indicated that the total energy converges to 2 meV/atom. The Pulay density mixing scheme was applied for the electron energy minimization process. The valence electronic configurations were Ag ($4d^{10}5s^{1}$), Ni ($3d^{8}4s^{2}$) in the calculations. After the structures are optimized, the total energies are recalculated self-consistently with the tetrahedron method.[17] The latter technique is also used to calculate the electronic density of states (DOS). Finally, the phonon spectrum and phonon density of states of the ground-state structure of the alloy are calculated based on the density functional perturbation theory (DFPT).[18]

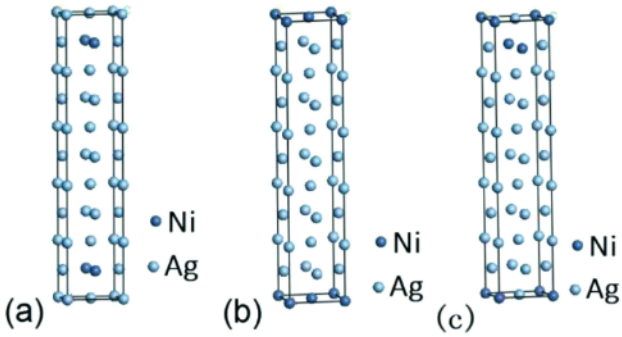

Figure 1: $AgNi_{10}$ solid-solution structure model with different Ni site: a) Ni1-model, b) Ni2-model, c) Ni3-model

The $5 \times 1 \times 1$ supercells of the $AgNi_{10}$ solid solution alloy investigated in this study were constructed mainly based on the pure Ag structural model. The Ag has a cF4 crystal structure with the space group Fm-3m (No. 225) where the Ag atom is in the 4a (0,0,0) Wyckoff site. The reported lattice parameter is 0.410 nm.[19] The tetragonal $5 \times 1 \times 1$ supercell contains 20 atoms. The different lattice positions of the 4a Wyckoff site in a Ag supercell of $5 \times 1 \times 1$ are substituted by two Ni atoms. In order to investigate the effect of the Ni site on the stability of $AgNi_{10}$ solid solution alloy, three structure models with different Ni site, i.e., Ni1, Ni2, Ni3, are constructed, as shown in **Figure 1.** The Ni1-model denotes that the two Ni atoms substitute for the Ag atoms located at face-centered sites in the fcc lattice. The Ni2-model denotes that the one Ni atom substitutes for the Ag atom located at face-centered and vertex sites in the fcc lattice, respectively. The Ni3-model denotes that the one Ni atom substitutes for the other Ag atom located at the face-centered and vertex sites in the fcc lattice, respectively.

3 RESULTS AND DISCUSSION

3.1 Crystal structures and stability

In the present work, the structural optimization was first performed by full relaxation of cell shape and atomic positions. The optimized lattice parameters are listed in **Table 1**. It was found that the substitution of the Ni atom for the Ag atom results in the increase of lattice parameters along with the *a* and *b* crystal orientation. This might occur because the supersaturated solid solution of Ni in Ag causes a large lattice stress, which leads to lattice distortion of the $AgNi_{10}$ supercell. Moreover, the space group of the Ni3-model changes from the tetragonal structure to the orthogonal structure. It is indicated that the occupation of Ni in Ag lattice has an important effect on the structural transformation of the supersaturated solid solution $AgNi_{10}$ alloys. At present, there are few reported experimental and theoretical stud-

Table 1: Calculated lattice parameters and the total energy for three $AgNi_{10}$ structure models

Models	Space group	*a*/nm	*b*/nm	*c*/nm	Cell volume (nm^3)	Total energy (eV/atom)
Supercell Ag	P4/mmm	0.4086	0.4086	2.043	0.341012	-20556.40
Ni1-model	P4/mmm	0.4145	0.4145	2.0146	0.346158	-21225.25
Ni2-model	P4/mmm	0.4120	0.4120	2.0230	0.343392	-21225.84
Ni3-model	Pmma	0.4128	0.4165	2.0133	0.346056	-21225.47

ies on Ag-Ni solid-solution alloys. We calculate the total energy of three $AgNi_{10}$ structure models, as shown in **Table 1**. It was found that the Ni2-model has lowest ground-state energy with respect to the Ni1-model and the Ni3-model, indicating that Ni occupies the sites in a Ag lattice to form an ordered structure. Generally, the more negative the energy is, the more stable is the corresponding crystal structure. The results have shown that the Ni2-model is a most stable $AgNi_{10}$ alloy.

3.2 Electronic structures

In the present work, the electronic structures were calculated to gain a further insight into the bonding of Ag-Ni alloys, and then to reveal the underlying structural stability mechanism of these alloys. The total density of states (TDOS) and partial density of states (PDOS) of the three models are presented in **Figure 2**. From **Figure 2** it can be that the TDOS plots are divided into three energy regions:

1. The low-energy region located from –8 eV to –2 eV, the lowest region stemming mainly from Ag-4d, Ag-5s and Ni-3d states.
2. The valence region located from –2 eV to 0 eV, the upper region of the valence band is cut by the Fermi level and is mainly due to valence electron numbers of Ni-3d mixed with Ag-4p states.
3. The unoccupied state: the energy region just above the Fermi level dominated by Ag-4p and Ag-5s states.

It can be easily found that TDOS in the low-energy region and valence region for Ni2-model lower than that of Ni1-model and Ni3-model. It is further revealed that the number of bonding electrons at the Fermi level for the Ni2-model decreases, indicating that the stability of the crystals increases, which corresponds well to the variation in cohesive energies of the models mentioned above. Moreover, by analyzing the bonding electron number of per atom in Region 2, 9.29 for the Ni1-model, 5.75 for Ni2-model, 11.08 for Ni3-model, respectively. It can be found that the bonding electron numbers per atom at the Fermi level in Region 2 for Ni2-model is smaller than that of Ni1-model and Ni3-model, respectively. This also indicates that the stability of the Ni2-model increases in comparison with the Ni1-model and the Ni3-model. Thus, we can draw a conclusion that different levels of stability between these structure models could be attributed to the bonding electron numbers (the majority being Ni-3d electrons) at the upper region of the

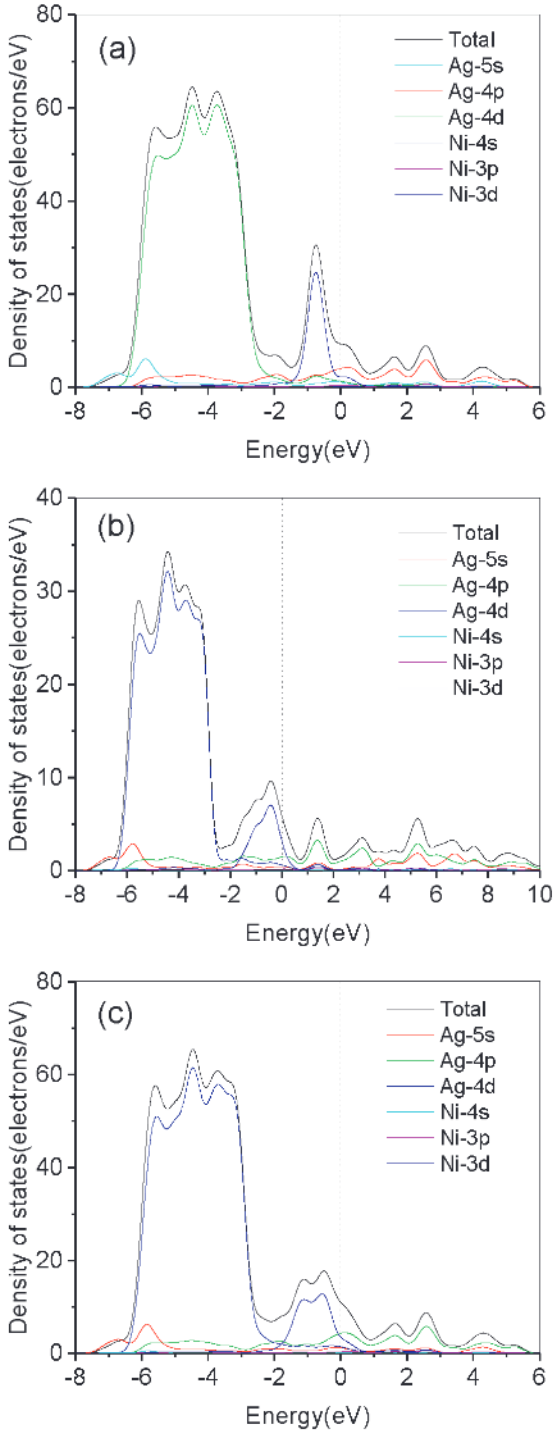

Figure 2: Calculated density of state (DOS): a) Ni1-model, b) Ni2-model, c) Ni3-model

Table 2: Calculated elastic constants, C_{ij} (GPa) for $AgNi_{10}$ structure models

Models	C_{11}	C_{12}	C_{13}	C_{22}	C_{23}	C_{33}	C_{44}	C_{55}	C_{66}
Ni1-model	108.16	81.94	116.74	–	–	102.24	59.08	–	42.21
Ni2-model	166.63	49.91	89.03	–	–	79.47	35.15	–	8.79
Ni3-model	85.82	67.24	91.42	80.98	86.04	69.76	61.66	29.33	23.26

valence band that is cut by the Fermi level (valence region).

3.3 Elastic constants and mechanical stability

Elastic constants are the measure of the resistance of a crystal to an externally applied stress. Through imposing a small strain on the perfect lattice, the elastic constants can be obtained. For the tetragonal Ni1-model and Ni2-model crystals, there are six independent elastic constants. For the orthorhombic Ni3-model crystal, there are nine independent elastic constants. The calculated elastic constants at the ground states are listed in **Table 2**.

The intrinsic mechanical stability of a solid is, in general, determined by certain conditions related to the crystal symmetry. The mechanical stabilities of the three $AgNi_{10}$ models have been analyzed according to the elastic constants. For different crystals, the elastic constants need to satisfy the generalized stability criteria: $C_{11} > 0$, $C_{33} > 0$, $C_{44} > 0$, $C_{66} > 0$, $C_{11} > C_{12}$, $C_{11} + C_{33}$-$2C_{13} > 0$, $2C_{11} + C_{33} + 2C_{12} + 4C_{13} > 0$ for tetragonal crystals;[20] $C_{11} > 0$, $C_{22} > 0$, $C_{33} > 0$, $C_{44} > 0$, $C_{55} > 0$, $C_{66} > 0$, $C_{11} + C_{22}$-$2C_{12} > 0$, $C_{11} + C_{33}$-$2C_{13} > 0$, $C_{22} + C_{33}$-$2C_{23} > 0$, $C_{11} + C_{22} + C_{33} + 2C_{12} + 2C_{13} + 2C_{23} > 0$ for orthorhombic crystals.[21] It is obvious that, from **Table 2**, all the elastic constants of the Ni2-model crystals meet the corresponding crystal's mechanical stability criteria, indicating that the $AgNi_{10}$ alloy with the Ni2-model structure is mechanically stable. While the Ni1-model and Ni3-model crystals do not meet the tetragonal and orthorhombic mechanical stability criteria, respectively. This reveals that $AgNi_{10}$ alloys with the Ni1-model and Ni3-model structures are mechanically metastable. Therefore, in the subsequent calculation of polycrystalline mechanical properties, only the Ni2-model with a stable structure is used.

The elastic properties of the polycrystalline materials are usually characterized by the elastic moduli, such as bulk modulus (B), Young's modulus (E), shear modulus (G) and Poisson's ratio (ν). On the basis of the approximations by Voigt[22] and Reuss,[23] Voigt bound (V) is obtained by the average polycrystalline moduli is based on an assumption of uniform strain throughout a polycrystal and is the upper limit of the actual effective moduli, while the Reuss bound (R) is obtained by assuming a uniform stress and is the lower limit of the actual effective moduli. For the tetragonal lattices, the Voigt bulk modulus (B_V) and shear modulus (G_V) are defined in Equations (1) and (2).

$$B_V = \frac{1}{9}(2C_{11} + 2C_{12} + C_{33} + 4C_{13}) \quad (1)$$

$$G_V = \frac{1}{15}(2C_{11} + C_{33} - C_{12} - 2C_{13} + 6C_{44} + 3C_{66}) \quad (2)$$

and the Reuss bulk modulus (B_R) and Reuss shear modulus (G_R) are defined in Equations (3) and (4).

$$B_R = \frac{1}{2S_{11} + S_{33} + 2S_{12} + 4S_{13})} \quad (3)$$

$$G_R = \frac{15}{4(2S_{11} + S_{13}) - 4(S_{12} + 2S_{13}) + (2S_{44} + S_{66})} \quad (4)$$

Using energy considerations, Hill proved that the Voigt and Reuss equations represent the upper and lower limits of the true polycrystalline constants, and recommended that a practical estimate of the bulk and shear moduli were the arithmetic means of the extremes.[24] The Hill's average or Voigt-Ruess-Hill approximation for the shear moduli (G_H) and bulk moduli (B_H) is given by Equations (5) and (6).

$$B_H = \frac{B_V + B_R}{2} \quad (5)$$

$$G_H = \frac{G_V + G_R}{2} \quad (6)$$

From B_H and G_H, the Young's modulus E and Poisson's ratio have been calculated using Hill's empirical average and the Equations (7) and (8).[25]

$$E = \frac{9B_H G_H}{(3B_H + G_H)} \quad (7)$$

$$\nu = \frac{(3B_H - 2G_H)}{(6B_H + 2G_H)} \quad (8)$$

The lame modulus (λ) is related to the bulk modulus (B_H) and the shear modulus (G_H) by the Equation (9).

$$\lambda = B_H - \frac{2}{3}G_H \quad (9)$$

The Kleinman parameter, ξ, describes the relative positions of the cation and anion under volume-conserving strain distortions for which positions are not fixed by symmetry. If there is a large resistance against bond bending or bond-angle distortion, the value of ξ is low and if otherwise, the value of ξ is high.[26,27] Kleinman parameter using the single-crystal elastic stiffness constants is calculated withe Equation (10).

$$\xi = \frac{C_{11} + 8C_{12}}{7C_{11} + 2C_{12}} \quad (10)$$

Table 3: Calculated bulk modulus (B), shear modulus (G), Young's modulus (E), B/G, Poisson's ratio (ν), lame modulus (λ), Kleinman's parameter (ξ) for the $AgNi_{10}$ structure model

B_V/GPa	B_R/GPa	B_H/GPa	G_V/GPa	G_R/GPa	G_H/GPa	E/GPa	ν	λ/GPa	ξ	B/G	$C1$	$C2$
107.61	70.05	88.33	28.14	9.99	19.07	53.36	0.399	76.12	0.447	4.66	41.12	53.87

The calculated bulk modulus (B_R, B_V, B_H), shear modulus (G_R, G_V, G_H), Young's modulus E, lame modulus (λ), Poisson's ratio (ν) and Kleinman's parameter (ξ) for the Ni2-model are given in **Table 3**. However, there are no theoretical and experimental reported values of the mechanical properties for the $AgNi_{10}$ alloy in the literature.

The ratio of the bulk modulus to the shear modulus of crystalline phases, proposed by Pugh,[28] can empirically predict the brittle and ductile behaviour of materials. A high B/G ratio is associated with ductility, whereas a low value corresponds to a brittle nature. The critical value which separates ductile and brittle material is around 1.75. The calculated B/G value for the $AgNi_{10}$ alloy is 4.59 (**Table 3**). It shows that the $AgNi_{10}$ alloy exhibits good ductility. Besides B/G, the ductility behaviour was also proposed to be related to the so-called Cauchy pressures.[29] For phases with tetragonal symmetry, the Cauchy pressures are defined in Equations (11) and (12).

$$C1 = C_{12} - C_{66} \tag{11}$$

$$C2 = C_{13} - C_{44} \tag{12}$$

Positive or negative values of $C1$ and $C2$ indicate ductile or brittle behaviour, respectively. The calculated values of $C1$ and $C2$ were shown in **Table 3**. It can be seen that both $C1$ and $C2$ of the $AgNi_{10}$ alloy are positive, indicating a ductile nature for the $AgNi_{10}$ alloy. Moreover, the ductility or brittleness behaviour can be characterized using Poisson's ratio (ν) according to criteria $\nu < 1/3$ for brittle materials and $\nu > 1/3$ for ductile materials.[30] Our calculated value of the Poisson's ratio (0.398) is remarkably larger than 1/3. Poisson's ratio is associated with the volume change during uniaxial deformation. If $\nu = 0.5$, no volume change occurs during elastic deformation. The low ν value for $AgNi_{10}$ means that a considerable volume change is associated with its deformation.

3.4 Elastic anisotropy

The elastic constants of solids are very important because they are closely associated with the mechanical and physical properties. In particular, they play an important role in providing valuable information about the structural stability and anisotropic characteristics.

The universal elastic anisotropy index A^U for crystals with any symmetry is proposed in Equation (13).[31]

$$A^U = 5\frac{G_V}{G_R} + \frac{B_V}{B_R} - 6 \geq 0 \tag{13}$$

To distinguish the shear and the bulk contributions to elastic anisotropy, The percentage anisotropy in compressibility (A_B) and shear (A_G) are defined in Equations (14) and (15).[32]

$$A_B = \frac{B_V - B_R}{B_V + B_R} \tag{14}$$

$$A_G = \frac{G_V - G_R}{G_V + G_R} \tag{15}$$

For all these indexes, a value of zero represents the elastic isotropy (isotropic structure) and the deviation from zero represents the anisotropic mechanical properties. The deviation of A^U from zero defines the extent of the single crystal anisotropy (i.e., the larger A^U represents the more anisotropic) and accounts for both the shear and the bulk contributions, unlike A_B and A_G.

The elastic anisotropy of the crystal is closely correlated with the possibility to induce microcracks and dislocations in the materials.[33,34] The shear resistance of the crystal (the energy change in a crystal associated with the shear modes along different slip directions) is characterized by the elastic anisotropy factors. In the tetragonal crystal, the anisotropic behaviour can be described by elastic anisotropy factors (Equations (16), (17) and (18)).

$$A_1 = \frac{2C_{66}}{(C_{11} - C_{12})} \tag{16}$$

$$A_2 = \frac{4C_{44}}{(C_{11} + C_{33} - 2C_{13})} \tag{17}$$

$$A_3 = \frac{C_{44}}{C_{66}} \tag{18}$$

A_1, A_2 and A_3 correspond to the {001} shear plane along the direction, the {011} shear plane along the direction and {100} shear plane along the d direction, respectively. For an anisotropic crystal the factors A_1, A_2 and A_3 must be unity. The deviation of the anisotropic factors from unity is a measure of the elastic anisotropy. The various anisotropy index value are shown in **Table 4**. The values of A_1, A_2, A_3 are significantly different from 1, indicting anisotropic. Also, the value of A_B, A_G and A^U deviate completely from zero (**Table 4**), which is much different from isotropic materials.

Table 4: Calculated universal anisotropic index A^U, percent anisotropy A_B and A_G, shear anisotropic factors (A_1, A_2, and A_3)

A^U	A_B	A_G	A_1	A_2	A_3
9.63	0.211	0.476	0.151	2.066	4.00

The anisotropy of elastic moduli can best be visualized by plotting them in three-dimensional surface showing their variation with respect to the direction. For the

tetragonal symmetry crystal, the directional dependence of the Young's modulus (E) and bulk modulus (B) is given by Equations (19) and (20).[35]

$$\frac{1}{B} = (S_{11} + S_{12} + S_{13})(l_1^2 + l_2^2) + (2S_{13} + S_{33})l_3^2 \quad (19)$$

$$\frac{1}{E} = S_{11}(l_1^4 + l_2^4) + S_{33}l_3^4 + (2S_{12} + S_{66})l_1^2 l_2^2 + (2S_{13} + S_{44})(l_1^2 l_3^2 + l_2^2 l_3^2) \quad (20)$$

where S_{ij} are the elastic compliance constants, and l_1, l_2 and l_3 are the directional cosines to the X, Y and Z axes under spherical coordinates, respectively. l_1, l_2 and l_3 can be obtained by $l_1 = \sin[\theta]\cos[\varphi]$, $l_2 = \sin[\theta]\sin[\varphi]$ and $l_3 = \cos[\theta]$ in spherical coordinates. The angles θ and φ are well defined in spherical coordinates.

In this representation, an isotropic system would have a spherical shape, and so the degree of deviation of the geometry from a sphere indicates the degree of anisotropy in a specific property of system. The representations on the directional dependence of B and E of both $AgNi_{10}$ show clear deviations from a spherical shape, as shown in **Figure 3** and **Figure 4**, respectively. The surface in each of the graphs represents the magnitude of B or E along different orientations. From the graphs, we can clearly see that the Young's modulus shows strong anisotropy for different orientations. On the other hand, the anisotropic property of bulk modulus of $AgNi_{10}$ is less prominent than the Young's modulus. This agrees with the calculated results of elastic anisotropic index A^U and elastic anisotropy ratios A_1, A_2, and A_3 in **Table 3**.

3.5 Thermodynamic properties

The Debye temperature θ_D is a fundamental attribute of a solid connecting the elastic properties with thermodynamic properties such as specific heat, sound velocity and melting temperature. It can be calculated from the averaged sound velocity, v_m by Equation (21).[36]

$$\theta_D = \frac{h}{k_B}\left[\frac{3n}{4\pi}\left(\frac{N_A\rho}{M}\right)\right]^{\frac{1}{3}} v_m \quad (21)$$

where h is Planck's constant, k_B is Boltzmann's constant, N_A is Avogadro's number, n is the number of atoms in the unit cell, M is the molecular weight and ρ is the density. The average sound velocity in the polycrystalline material is approximately given by Equation (22).[36]

$$v_m = \left[\frac{1}{3}\left(\frac{2}{v_s^3} + \frac{1}{v_l^3}\right)\right]^{-\frac{1}{3}} \quad (22)$$

where v_l and v_s are the longitudinal and transverse sound velocity, respectively, which can be obtained using the shear modulus G and the bulk modulus B from Navier's Equations (23).[37]

$$v_l = \sqrt{\frac{B + 4G/3}{\rho}} \text{ and } v_s = \sqrt{\frac{G}{\rho}} \quad (23)$$

The calculated values of the sound velocity and Debye temperature as well as the density for the $AgNi_{10}$ are given in **Table 5**. From **Table 5** we see that the Debye temperature calculated using single-crystal elastic constants is 378 K.

Table 5: Calculated density (ρ), the longitudinal, transverse, and average sound velocity (v_l, v_s, v_m), the Debye temperatures (θ_D) and the melting temperature (T_m)

v_l/ (m·s^{-1})	v_s/ (m·s^{-1})	v_m/ (m·s^{-1})	ρ/ (kg·m^{-3})	θ_D/K	T_m/K
3089	3006	3378	11910	378	1173

The melting temperature is considered to be an important index to evaluate the heat resistance of alloy materials. For tetragonal structural metals, the melting temperature, T_m can be expressed as Equation (24).[38]

$$T_m = 254\text{K} + \left(\frac{4.50\text{K}}{\text{GPa}}\right)\left[\frac{1}{3(2C_{11} + C_{33})}\right] + 300\text{K} \quad (24)$$

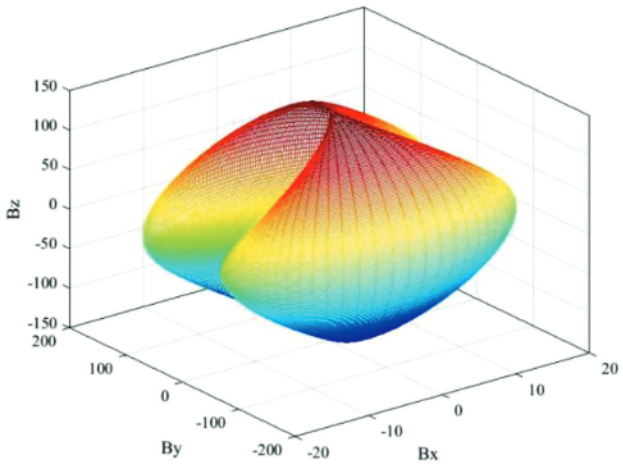

Figure 3: Directional dependence of bulk modulus in $AgNi_{10}$

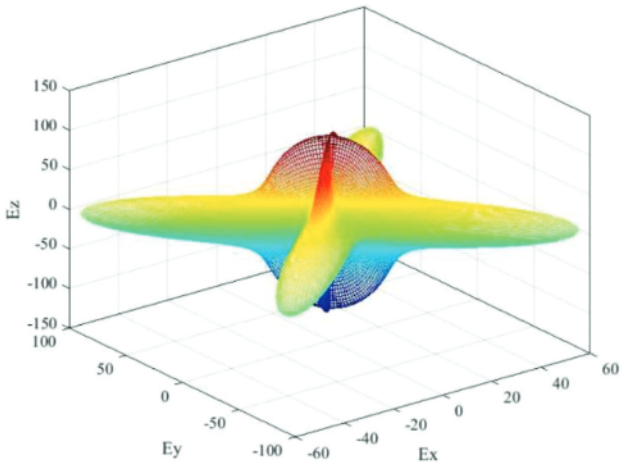

Figure 4: Directional dependence of Young's modulus in $AgNi_{10}$

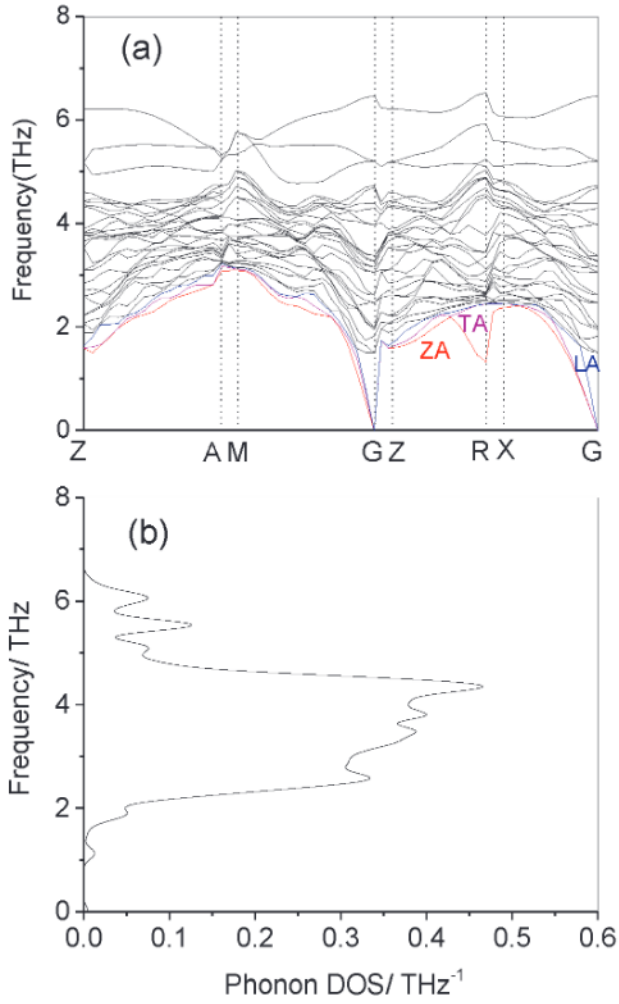

Figure 5: Phonon dispersions and Phonon DOS of $AgNi_{10}$: a) Phonon dispersions, b) Phonon DOS

The calculated value of the melting temperature for $AgNi_{10}$ is 1173 K (**Table 5**).

Figure 5a shows first-principles calculated phonon dispersion curves of $AgNi_{10}$ along high-symmetry points of the P4/mmm BZ, where no imaginary frequencies in the whole Brillouin zone and do not show any anomaly for all the phonon modes, confirming that $AgNi_{10}$ with a tetragonal structure is dynamically stable. The three branches in the low-frequency region where the frequency is zero at point G in the center of Brillouin zone, are ZA, TA and LA. The ZA is the flexural acoustic mode with the atomic vibrations along the perpendicular (Z) direction; the LA and TA are the longitudinal and transverse acoustic modes, respectively, with the atomic vibrations both in the XY plane. The frequency order for the acoustic modes is ZA < TA < LA. The other branches are optical modes with higher frequencies. The phonon density of states (PhDOS) for $AgNi_{10}$ is shown in **Figure 5b**. The vibration mode in the crystal mainly appears in the low-frequency region (2–5 THz), and there is a maximum peak at the frequency of 4.36 THz, indicating that the lattice vibration of the $AgNi_{10}$ crystal is relatively concentrated near this frequency.

In the approximation of the Debye model, the heat capacity at constant volume of the solid, C_v can be obtained from the Debye temperature by Equation (25).[39]

$$C_V = 9N_A k_B \left(\frac{T}{\theta_D}\right)^3 \int_0^{\theta_D/T} \frac{x^4 e^x}{(e^x - 1)^2} dx \qquad (25)$$

where T is the temperature (K).

The calculated values of C_v for $AgNi_{10}$ are shown in **Figure 6**. One can easily see that C_v increases rapidly with the increase of temperature below θ_D. Namely, the variation of C_v is dependent on the temperature at low temperature. At the same time at sufficiently low temperatures ($T < \theta_D$), C_v is approximately proportional to T^3.[40] However, the anharmonic effect on C_v is suppressed at higher temperature ($T > \theta_D$), the heat capacity C_v approaches to a constant Dulong–Petit limit $3nN_Ak_B$ ($\approx$ 249.43 J/mol·K) where n = 10 is number of atoms for $AgNi_{10}$ primitive cell, N_A is the Avogadro number and K_B is the Boltzmann's constant. At intermediate temperatures, the temperature dependence of C_v is governed by the details of vibrations of the atoms.

We also plotted the change of entropy, the free energy and enthalpy with temperature in **Figure 7** for $AgNi_{10}$. It can be seen that the entropy increases quickly with increasing temperature. It is consistent with common sense, because the entropy of a crystal is generated by lattice vibrations and electronic excitation, and as the temperature goes up, the lattice vibrations of the crystal increases and the electrons are more likely to be excited. The free energy of $AgNi_{10}$ decreases with an increase of temperature. The decrease of free energy is the driving force of crystal phase transition ($F = U - TS$, where F, U, S is free energy, internal energy and entropy, respectively). With the increase of temperature, the internal energy in the system increases, and the entropy of the system increases, but the speed of the TS increase is greater than that of U, so the free energy of the crystal decreases

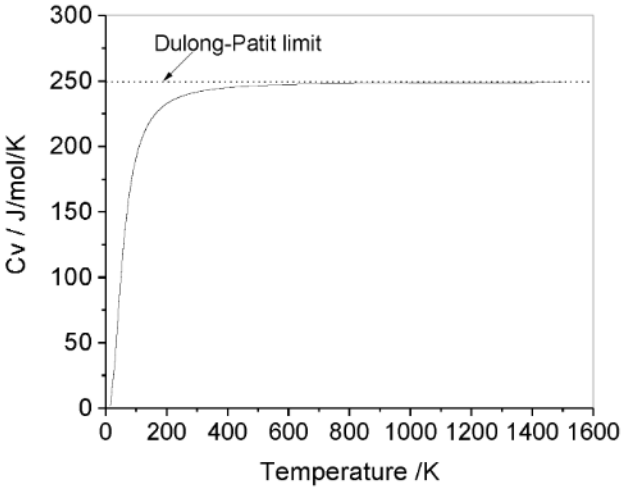

Figure 6: Dependence of specific heat on temperature for $AgNi_{10}$

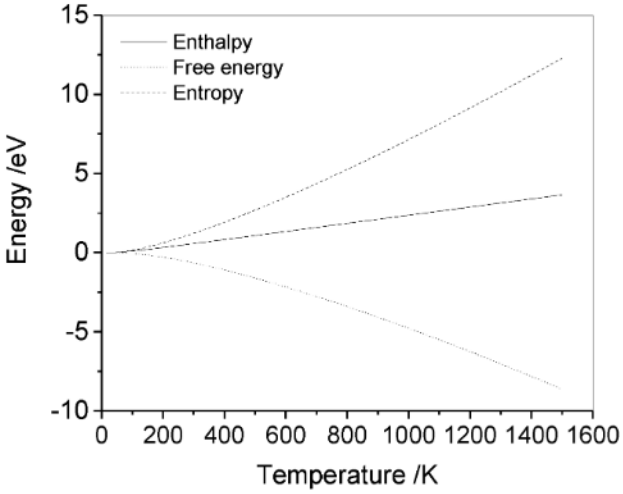

Figure 7: Dependence of the entropy, enthalpy and free energy on temperature for $AgNi_{10}$

with the increase of temperature. Enthalpy of $AgNi_{10}$ increases the increase of temperature. The meaning of enthalpy is that the enthalpy of the system is equal to the heat absorbed by the crystal under isobaric conditions ($H = U - PV$, where P, V is pressure and volume, respectively). With the increase of temperature, the internal energy of the system increases, and the crystal expands thermally, resulting in the PV increases. Therefore, the enthalpy of the crystal increases with the increase of the temperature.

4 CONCUSIONS

The structural, electronic, elastic and thermodynamic properties of $AgNi_{10}$ were studied by employing the pseudo-potential plane-wave approach based on density functional theory, within the GGA functional. The calculated structural and electronic properties of a supersaturated solid solution of $AgNi_{10}$ alloys show that the occupation of Ni in the Ag lattice is ordered. The energetically and mechanically optimized stable $AgNi_{10}$ model is that the one Ni atom substitutes for the Ag atom located at face-centered and vertex sites in fcc lattice. All single-crystal elastic stiffness constants are calculated using the finite strain method and using the Voigt–Reuss–Hill approximation, value of the ideal polycrystalline aggregates bulk modulus (83.33 GPa), shear modulus (19.07 GPa), Young's modulus (53.36 GPa), and Poisson's ratio (0.399), are obtained. The calculated B/G and Cauchy pressure values show that $AgNi_{10}$ behaves in a ductile manner. Anisotropy in the elastic properties was studied by computing various anisotropic indices and the directional dependence of B and E. The strong anisotropy in the elastic properties of $AgNi_{10}$ was confirmed. Phonon dispersions were carried out, and showed that the $AgNi_{10}$ crystal has dynamic stability. The Debye temperature is calculated from the elastic data by estimating the average sound velocity in the $AgNi_{10}$. Furthermore, the vibrational thermodynamic properties (free energy, enthalpy, entropy and heat capacity) of $AgNi_{10}$ are obtained successfully.

Acknowledgment

This work was supported by the genetic engineering of rare and precious metal materials in Yunnan Province (202002AB080001-1); Shenyang Young and Middle-aged Science and Technology Innovation Talents Project (RC200355) in Liaoning Province, China; Innovation talent Project of colleges and universities in Liaoning Province in 2020.

5 REFERENCES

[1] P. Verma, O. P. Pandey, A. Verma, Influence of metal oxides on the arc erosion behaviour of silver metal oxides electrical contact materials, Journal of Materials Science & Technology, 20 (**2004**)1, 49–52

[2] H. F. Yu, J. X. Lei, X. M. Ma, L. H. Zhu, Y. Lu, J. Xiang, W. Weng, Application of nanotechnology in a silver/graphite contact material and optimization of its physical and mechanical properties, Rare Metals , 23 (**2004**) 1, 79–83, CNKI:SUN:XYJS.0.2004-01-025

[3] F. Chen, Y. Feng, H. Shao, Friction and wear behaviours of Ag/MoS2/G composite in different atomspheres and at different temperatures, Tribology Letters, 47 (**2012**) 1, 139–148, doi:10.1007/s11249-012-9970-3

[4] B. Rehani, P. B. Joshi, P. K. Khanna, Fabrication of silver-graphite contact materials using silver nanopowders, Journal of Materials Engineering and Performance, 19 (**2010**) 1, 64–69, doi:10.1007/s11665-009-9437-3

[5] T. B. Massalski, H. Okamoto, P. R. Subramanian, Binary Alloy Phase Diagrams, 2nd ed., ASM International, Materials Park, OH, 1990, 64–66

[6] F. R. de Boer, R. Boom, W. C. M. Mattens, Cohesion in Metals. North-Holland, Amsterdam, 1988, 95–98

[7] R. P. van Ingen, R. H. J. Fastenau, E. J. Mittemeijer, Formation of Crystalline AgxNi1-x solid solutions of unusually high supersaturation by laser ablation deposition, Physical Review Letters, 72 (**1994**), 3116–3119, doi:10.1103/PhysRevLett.72.3116

[8] J. W. Mayer, B. Y. Tsaur, S. S. Lau, Ion-beam-induced reactions in metal-semiconductor and metal-metal thin film structures, Nuclear Instruments and Methods, 182 (**1981**), 66–67, doi:10.1016/0029-554X(81)90666-2

[9] J. Xu, U. Herr, T. Klassen, Formation of supersaturated solid solution in the immiscible Ni-Ag system by mechanical alloying, J. Appl. Phys., 79 (**1996**), 3935–3945, doi:10.1063/1.361820

[10] J. H. He, E. Ma, Nanoscale phase separation and local icosahedral order in amorphous alloys of immiscible elements, Physical Review B, 64 (**2001**) 14, 144206, doi:10.1103/PhysRevB.64.144206

[11] J. H. He, H. W. Sheng, P. J. Schilling, C. L. Chien, E. Ma, Amorphous Structures in the Immiscible Ag-Ni System, Physical Review Letters, 86 (**2001**) 13, 2826–2829, doi:10.1103/PhysRevLett.86.2826

[12] J. A. Alonso, L. J. Gallego, J. A. Simozar, Construction of free-energy diagrams of amorphous alloys. Il Nuovo Cimento D, 12 (**1990**), 587–595, doi:10.1007/BF02453312

[13] http://www.pwscf.org

[14] D. Vanderbilt, Soft self-consistent pseudopotentials in a generalized eigenvalue formalism, Physical Review B, 41 (**1990**) 13, 7892–7895, doi:10.1103/PhysRevB.41.7892

[15] J. P. Perdew, Y. Wang, Accurate and simple analytic representation of the electron-gas correlation energy, Physical Review B, 45 (**1992**) 23, 13244–13249, doi:10.1103/PhysRevB.45.13244

[16] H. J. Monkhorst, J. D. Pack, Special points for Brillouin-zone integrations, Physical Review B, 13 (**1976**) 13, 5188–5192, doi:10.1103/PhysRevB.13.5188

[17] N. I. Medvedeva, Y. N. Gornostyrev, D. L. Novikov, O. N. Mryasov, A. J. Freeman, Ternary site preference energies, size misfits and solid solution hardening in NiAl and FeAl, Acta Materialia, 46 (1998) 13, 3433–3442, doi:10.1016/S1359-6454(98)00042-1

[18] S. Baroni, P. Giannozzi, A. Testa, Green's-function approach to linear response in solids, Physical Review Letters, 58 (**1987**) 18, 1861–1864, doi:10.1103/PhysRevLett.58.1861

[19] R. P. van Ingen, R. H. J. Fastenau, E. J. Mittemeijer, Laser ablation deposition of Cu-Ni and Ag-Ni films: Nonconservation of alloy composition and film microstructure, Journal of Applied Physics, 76 (**1994**) 13, 1871, doi:10.1063/1.357711

[20] D. C. Wallace, Thermodynamics of Crystal, Wiley, New York, 1972

[21] O. Beckstein, J. E. Klepeis, G. L. W. Hart, O. Pankratov, First-principles elastic constants and electronic structure of α-Pt_2Si and PtSi, Physical Review B, 63 (**2001**) 13, 134112, doi:10.1103/PhysRevB.63.134112

[22] W. Voigt, Lehrbuch der Kristallphysik, Teubner, Leipzig, 1928

[23] A. Reuss, Berchung der Fiessgrenze von Mischkristallen auf Grund der Plastiziä tsbedingung für Einkristalle Z, Angew Math Mech, 9 (**1929**), 49, doi: 10.1002/(ISSN)1521-4001

[24] R. Hill, The elastic behaviour of a crystalline aggregate, Proc. Phys. Soc., London, Sect. A, 65 (**1952**), 349–354, doi:10.1088/0370-1298/65/5/307

[25] A. M. Hao, X. C. Yang, X. M. Wang, Y. Zhu, X. Liu, R. P. Liu, First-principles investigations on electronic, elastic and optical properties of XC (X=SiX=Si, Ge, and Sn) under high pressure, J. Appl. Phys, 108 (2010), 063531, doi:10.1063/1.3478717

[26] K. Kim, W. R. L. Lambrecht, B. Segal, Electronic structure of GaN with strain and phonon distortions, Physical Review B, 50 (**1994**) 3, 1502–1505, doi:10.1103/PhysRevB.50.1502

[27] L. Kleinman, Deformation Potentials in Silicon. I. Uniaxial Strain, Physical Review B, 128 (**1962**) 4, 2614–2621, doi:10.1103/PhysRev.128.2614

[28] S. F. Pugh, XCII. Relations between the elastic moduli and the plastic properties of polycrystalline pure metals, Philosophical Magazine, 45 (**1954**) 367, 823–843, doi:10.1080/14786440808520496

[29] D. G. Pettifor, M. Aoki, Bonding and structure of intermetallics: a new bond order potential, Philosophical Transactions of the Royal Society A, 334 (**1991**) 1635, 439–449, doi:10.1098/rsta.1991.0024

[30] I. N. Frantsevich, F. F. Voronov, S. A. Bokuta, in: I. N. Franstsevich (Ed.), Elastic Constants and Elastic Moduli of Metals and Insulators Handbook, Kiev, Naukova Dumka, 1983, 60–180

[31] S. I. Ranganathan, M. Ostoja-Starzewski, Universal Elastic Anisotropy Index, Physical Review Letters, 101 (**2008**) 5, 055504, doi:10.1103/PhysRevLett.101.055504

[32] D. H. Chung, W. R. Buessem, in: F.W. Vahldiek, S.A. Mersol (Eds.), Anisotropy in Single Crystal Refractory Compound, Plenum, New York, 1968, 217

[33] J. R. Rice, Dislocation nucleation from a crack tip: An analysis based on the Peierls concept, Journal of the Mechanics and Physics of Solids, 40 (**1992**) 2, 239–271, doi:10.1016/S0022-5096(05)80012-2

[34] V. Tvergaard, J. W. Hutchinson, Microcracking in Ceramics Induced by Thermal Expansion or Elastic Anisotropy, Journal of the American Ceramic Society, 71 (**1988**) 3, 157–166, doi:10.1111/j.1151-2916.1988.tb05022.x

[35] J. F. Nye, Physical Properties of Crystals, Clarendon Press, Oxford, 1985

[36] O. L. Anderson, A simplified method for calculating the Debye temperature from elastic constants, J. Phys. Chem. Solids, 24 (**1963**) 7, 909–917, doi:10.1016/0022-3697(63)90067-2

[37] E. Schreiber, O. L. Anderson, N. Soga, Elastic constants and their measurements, McGraw-Hill, New York, 1973

[38] M. E. Fine, L. D. Brown, H. L. Marcus, Elastic constants versus melting temperature in metals, Scripta Metallurgica, 18 (**1984**) 9, 951–956, doi:10.1016/0036-9748(84)90267-9

[39] M. A. Blanco, E. Francisco, V. Luana, GIBBS: Isothermal-isobaric thermodynamics of solids from energy curves using a quasi-harmonic Debye model, Comput. Phys. Commun., 158 (**2004**), 57–72, doi:10.1016/j.comphy.2003.12.001

[40] J. P. Poirier, Introduction to the Physics of the Earth's Interior, Cambridge University Press, Oxford. 2000